Structure characteristics and mechanical properties of kaolinite soils. II. Effects of structure on mechanical properties

Y.-H. Wang and W.-K. Siu

Abstract: This paper reports the effects of structure on the mechanical responses of kaolinite with known and controlled fabric associations. The dynamic properties and strength were assessed by resonant column tests and undrained triaxial compression tests, respectively. The experimental results demonstrate that interparticle forces and associated fabric arrangements influence the volumetric change under isotropic compression. Soils with different structures have individual consolidation lines, and the merging trend is not readily seen under an isotropic confinement up to 250 kPa. The dynamic properties of kaolinite were found to be intimately related to the soil structure. Stronger interparticle forces or higher degrees of flocculated structure lead to a greater small-strain shear modulus, G_{max}, and a lower associated damping ratio, D_{min}. The soil structure has no apparent influence on the critical-state friction angle ($\phi'_c = 27.5°$), which suggests that the critical stress ratio does not depend on interparticle forces. The undrained shear strength of kaolinite is controlled by its initial packing density rather than by any interparticle attractive forces, and yet the influence of the structure on the effective stress path is obvious.

Key words: interparticle forces, shear modulus, damping ratio, stress–strain behavior, undrained shear strength, critical state.

Résumé : Cet article présente un rapport traitant des effets de structure sur les réponses de la kaolinite avec des associations de fabriques connues et contrôlées associées. Les propriétés dynamiques et la résistance ont été évaluées respectivement par des essais de colonnes résonnantes et des essais de compression triaxiale non drainée. Les résultats expérimentaux démontrent que les forces interparticules et les arrangements associés de fabrique influencent le changement volumétrique sous une compression isotrope. Les sols avec différentes structures ont des lignes de consolidation individuelles et la tendance à la fusion ne se voit pas facilement sous un confinement isotrope atteignant 250 kPa, On a trouvé que les propriétés dynamiques de la kaolinite étaient intimement reliées à la structure du sol. Des forces interparticules plus élevées ou de plus hauts degrés de floculation de structure conduisent à un plus grand module de cisaillement à faible déformation G_{max} et un plus faible rapport d'amortissement associé D_{min}. La structure du sol n'a pas d'influence apparente sur l'angle de frottement à l'état critique ($\phi'_c = 27.5°$), ce qui suggère que le rapport de contraintes critiques ne dépend pas des forces interparticules. La résistance au cisaillement non drainé de la kaolinite est contrôlée par sa densité de compactage initial plutôt que par quelque forces d'attraction interparticule. Par ailleurs, l'influence de la structure sur le cheminement des contraintes effectives est clair.

Mots clés : forces interparticules, module de cisaillement, rapport d'amortissement, comportement contrainte–déformation, résistance au cisaillement non drainé, état critique.

[Traduit par la Rédaction]

Introduction

The term structure when applied to fine-grained soils not only describes the geometrical arrangement of the particles (i.e., the soil fabric), but also implies the interparticle forces (Mitchell 1993). This is because the two factors are intimately correlated. The structure of a fine-grained soil is crucial to its engineering properties, and therefore the associated effects have been widely studied in terms of stiffness, strength, deformation characteristics, fabric anisotropy and alterations, and critical-state behavior. A review of the key findings in these areas is presented in Table 1. Guided by these important understandings and the fabric features revealed in the companion paper (Wang and Siu 2006), the aim of this study is to gain insights into how the mechanical responses of kaolinite soils are affected by different known and controllable structures. The intention is to elucidate the mechanical property implications of (*i*) the competitive effects between interparticle electrical forces and the applied state of stress; (*ii*) the dynamic properties, with a particular

Received 23 November 2004. Accepted 10 March 2006. Published on the NRC Research Press Web site at http://cgj.nrc.ca on 1 June 2006.

Y.-H. Wang[1] and W.-K. Siu. Department of Civil Engineering, Hong Kong University of Science and Technology, Clear Water Bay, Kowloon, Hong Kong.

[1]Corresponding author (e-mail: ceyhwang@ust.hk).

 doi:10.1139/T06-027

Table 1. Key findings concerning chemical–mechanical coupling in kaolinite clays.

Key findings	References
Deformation characteristics and fabric changes	
Soil with a flocculated structure has higher compressibility than soil with a dispersed structure under an applied stress greater than the preconsolidation pressure	Review in Mitchell 1993
The volume change is controlled by the interparticle resistance and double-layer repulsive forces	Sridharan and Venkatappa Rao 1973; Sridharan and Jayadeva 1982; review in Mitchell 1993
The larger inter-aggregate pores should be taken into account to explain deformation behavior not controlled by the double layer	Delage and Lefebvre 1983
An isotropic consolidation to a pressure of about two times the prior K_0 consolidation pressure can alter the strain responses to be isotropic; however, the fabric anisotropy remains, even after the material is subjected to subsequent much higher isotropic confinement, suggesting that isotropy is with respect to the cluster orientation rather than the particle alignment within clusters	Anandarajah et al. 1996; Kuganenthira et al. 1996
Particles tend to align perpendicular to the direction of loading during K_0 consolidation	Martin and Ladd 1978; Hicher et al. 2000; Yao and Anandarajah 2003
Stiffness and damping ratio	
The *S*-wave velocity decreases with an increase in ionic strength of KCl, which seems contrary to the prediction based on the Derjaguin–Landau–Verwey–Overbeek (DLVO) forces	Santamarina and Fam 1995
The soil structure can affect the shear modulus and damping ratio measured by resonant column testing	Edil and Luh 1980; Du et al. 1986
Strength and stress–strain behavior	
The friction angle ϕ' and cohesion intercept c increase with a decrease in the dielectric constant of the pore fluid	Sridharan and Venkatappa Rao 1979
The undrained shear strength changes with pore fluid with various dielectric constants	Moore and Mitchell 1974; Anandarajah and Zhao 2000
The undrained shear strength is governed by the interparticle forces and associated modes of particle arrangement; the strength and liquid limit demonstrate consistent trends	Sridharan and Prakash 1999
Specimens trimmed in the horizontal and vertical directions demonstrate identical stress–strain behavior in the triaxial tests	Ting 1968; Kuganenthira et al. 1996
Experimental results suggest that the anisotropic stress–strain behavior is controlled by cluster-to-cluster orientation rather than particle-to-particle orientation	Kuganenthira et al. 1996
Influence of compaction procedure on the mechanical behavior	
The soil structure shows no effects on the critical state in the q–p' plane but reveals an influence in the $e - \ln p'$ space (where e is the void ratio, p' is the mean effective stress, q is the deviatoric stress, and the compaction procedure means compaction water contents and types of compaction)	Wheeler and Sivakumar 2000

emphasis on the small-strain shear modulus G_{max} and associated damping ratio D_{min}; and (*iii*) the stress–strain response and critical-state behavior.

Material and sample preparation

The clay material used in this study, namely Speswhite Kaolin, is characterized in the companion paper (Wang and Siu 2006), which describes the soil properties, pretreatment procedures (washing), and methods of adjusting pore-fluid properties in the clay suspension.

One-dimensional (1D) consolidation and specimen trimming

The specimens used in the study of mechanical properties were prepared by K_0 consolidation of treated clay suspensions with a certain pore-fluid property under an effective vertical stress of 50 kPa (where K_0 is the lateral earth pressure coefficient at rest). The consolidation was considered finished when the recorded vertical settlement converged to a steady value. In general, the consolidation process lasted 1 week for samples with low pH and more than 1 month for high-pH samples. The consolidated clay was then carefully trimmed into designated sizes for testing using a tailor-made tube with a thin lubricated wall. The sample was 35 mm in diameter and 70 mm high for the resonant column test and 50 mm in diameter and 100 mm high for the undrained triaxial compression test. Most of the specimens were trimmed along the direction of the major principal stress (i.e., the direction of the vertical loading in the K_0 consolidation). Nevertheless, some specimens were also purposely trimmed along the minor principal stress direction. These specimens are denoted "minor" or "horizontal" samples in the following discussions. For clarification, Fig. 1 illustrates the directions in which the specimens were trimmed.

Installation and back-pressure saturation

A low vacuum pressure of ~20 kPa was applied during

Fig. 1. How vertical and horizontal specimens were trimmed after sample preparations by 1D consolidation (where σ'_v is the vertical effective stress, σ'_h is the horizontal effective stress, and K_0 is the lateral earth pressure coefficient at rest).

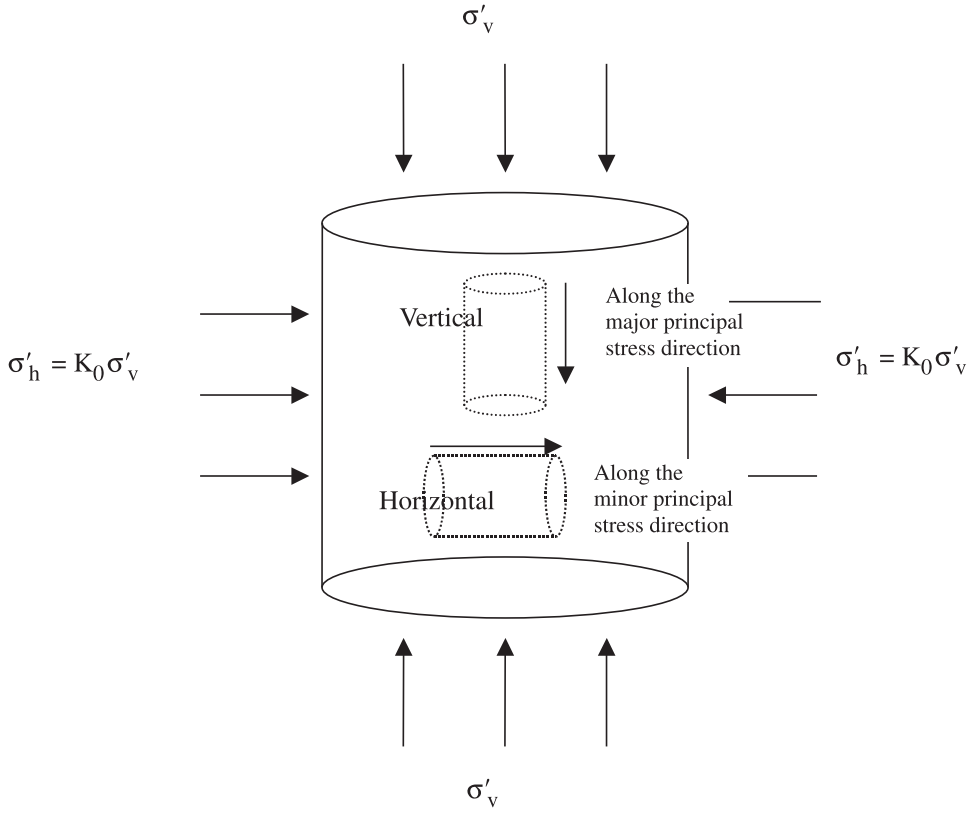

specimen installation into the testing device to minimize any disturbance of the soil structure. This low vacuum pressure was continuously applied until air bubbles entrapped at the specimen ends were removed, which took about 24 h. The diameter and height of the specimen were then measured as the initial values. The diameter of the specimen was gauged using a π tape with a resolution of 0.01 mm. The diameter at the top, middle, and bottom of the specimen was measured and an average value was taken. The height of the specimen was gauged using a vernier caliper with a resolution of 0.01 mm. After the outside chamber had been assembled, deaired water was allowed to flow in, and thus the whole specimen was immersed in water during saturation and consolidation to prevent air bubbles from diffusing into the specimen. Back-pressure saturation integrated with *B*-value checking was also implemented. A minimum back pressure of 200 kPa was applied in all tests; the soil specimen was regarded as fully saturated when the *B* value was greater than 0.98.

Experimental details

Resonant column tests and undrained triaxial compression tests were performed to investigate the effects of structure on the mechanical properties of the kaolinite.

Resonant column test

The resonant column tests were carried out by an energy-injecting virtual mass resonant column system (Li et al. 1998). The measurements were made under five different isotropic stress states ranging from 50 to 250 kPa in increments of 50 kPa. The maximum strain level was controlled to be less than 10^{-4} for each testing. At the last stage where the confining pressure was 250 kPa, the maximum applied strain was allowed to reach the equipment limit of ~0.002. The volumetric and axial strains in response to isotropic confinement were recorded for the purpose of characterizing the deformation behavior of soils with different fabric associations.

The experimental design of dynamic properties involves five different aspects. The first aspect considered is the pH effect. In the companion paper (Wang and Siu 2006), it was revealed that the isoelectrical point of the edge surfaces, IEP_{edge}, of Speswhite Kaolin is about 5. With increasing pH across this transition value, the fabric association can gradually change from edge-to-face (EF) flocculation to a deflocculated–dispersed structure. Consequently, pH 4, pH 5, and pH 7.8 specimens were prepared for investigation. Second, the influence of ionic strength is considered in which the behavior of pH 4 and pH 7.8 specimens was studied after the addition of 0.15 mol/L NaCl. The third aspect considered is fabric anisotropy. The properties of pH 4 and pH 7.8 specimens trimmed in the two perpendicular directions (illustrated in Fig. 1) were assessed. The fourth aspect is the effect of confining pressure (σ'_0) on the dynamic properties of the soil, with particular emphasis on the associated contact behavior in terms of modulus–stress power relationships. The fifth aspect is the normalized shear modulus degradation curves (G/G_{max}) and the damping-ratio curve (D/D_{min}) for samples with different fabrics under the same

Fig. 2. Volumetric changes (in terms of void ratios) of soils with different structures under isotropic compression.

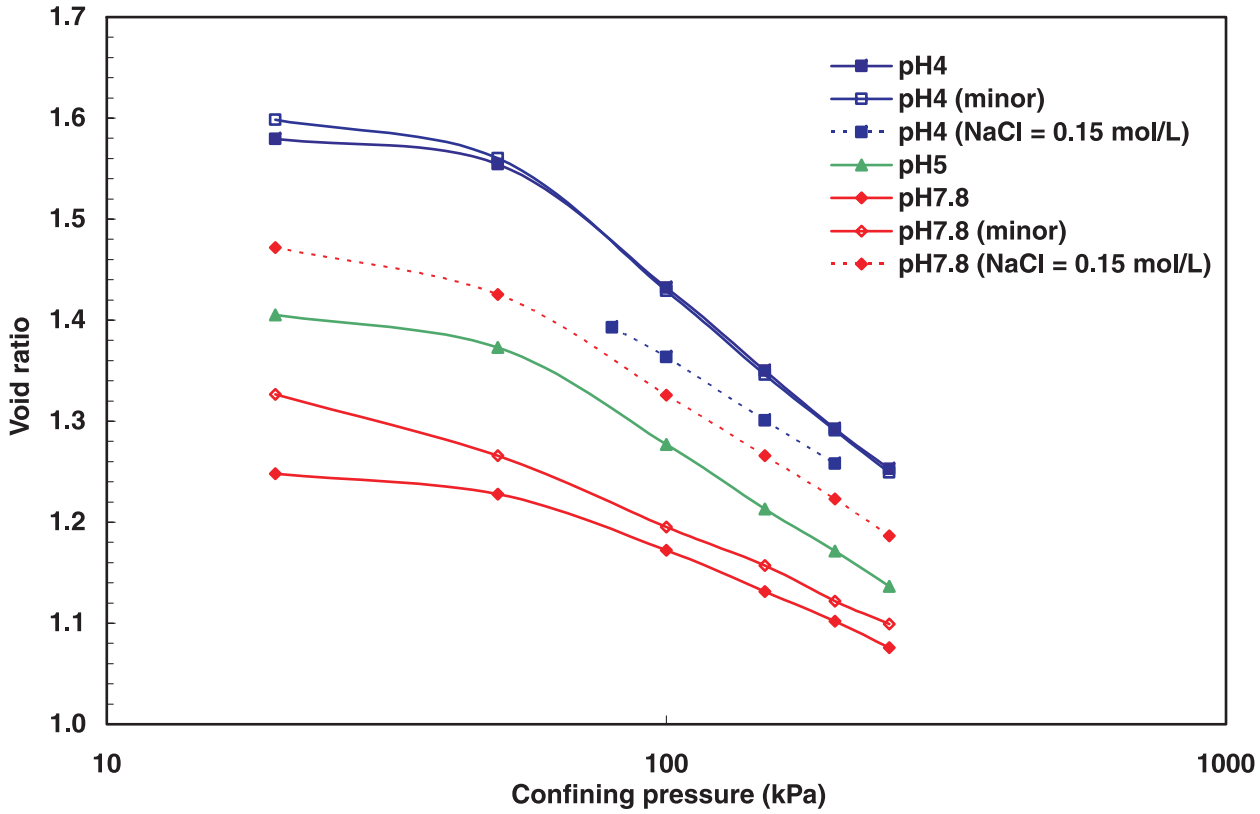

effective confinement (250 kPa). All of these curves were compared with the published empirical relations correlated with the plasticity index, PI.

Triaxial undrained compression test

The undrained triaxial compression tests were performed using a CKC triaxial system (Li et al. 1988). Based on the method suggested by Head (1994), a strain rate of 0.015%/min for applying the deviatoric stress is required for the specimens with the lowest permeability (i.e., the pH 7.8 specimens). This strain rate was adopted for all tests, thereby avoiding strain-rate effects. To erase the stress memory of K_0 consolidation imprinted during sample preparation, the minimum effective confining pressure in the tests was 100 kPa, which is twice the prior K_0 consolidation pressure. This value was chosen based on stable responses of volumetric strains to the isotropic confinement (shown later in the paper) and the experimental findings of Anandarajah et al. (1996). Samples with two representative fabric associations were selected for testing (i.e., pH 4 and pH 7.8 specimens). The changes in stress–strain behavior after adding 0.15 mol/L NaCl to the two samples were investigated as well.

Experimental results and discussion

Deformation characteristics under isotropic loading

A lengthy discussion of the prevailing interparticle forces and associated fabrics formed in different pore-fluid conditions is presented in the companion paper (Wang and Siu 2006) and thus is not repeated in the following discussions of experimental results.

Table 2. The compression index (C_c) of soils with different structures.

Pore fluid properties of soil sample	C_c
pH 4	0.453
pH 4 (minor)	0.452
pH 4 and [NaCl] = 0.15 mol/L	0.350
pH 5	0.352
pH 7.8	0.241
pH 7.8 (minor)	0.241
pH 7.8 and [NaCl] = 0.15 mol/L.	0.359

Note: The compression index C_c (= $\Delta e/\Delta(\log\sigma'_0)$) was determined at confining pressures greater than 100 kPa, which is twice the prior K_0 consolidation pressure used in the sample preparation.

Volume change under isotropic confinement

Figure 2 and Table 2 present the volume-change characteristics of soils with different fabric associations under isotropic confinement. It can be seen that the initial void ratio and compressibility (in terms of compression index C_c) are intimately related to the microstructure–fabric association. Although the edge-to-face (EF) flocculation dominates at lower pH, the samples possess larger void ratios and higher compressibility. On the other hand, denser specimens with lower compressibility are observed as the face-to-face (FF) alignment (or dispersed structure following the traditional

Fig. 3. Illustrations of volume-change mechanisms for soils with a flocculated structure, i.e., pH 4 (with less aggregated structures), pH 4 with salts, and pH 7.8 with salt specimens, and the face-to-face (FF) alignment, i.e., the 7.8 specimen.

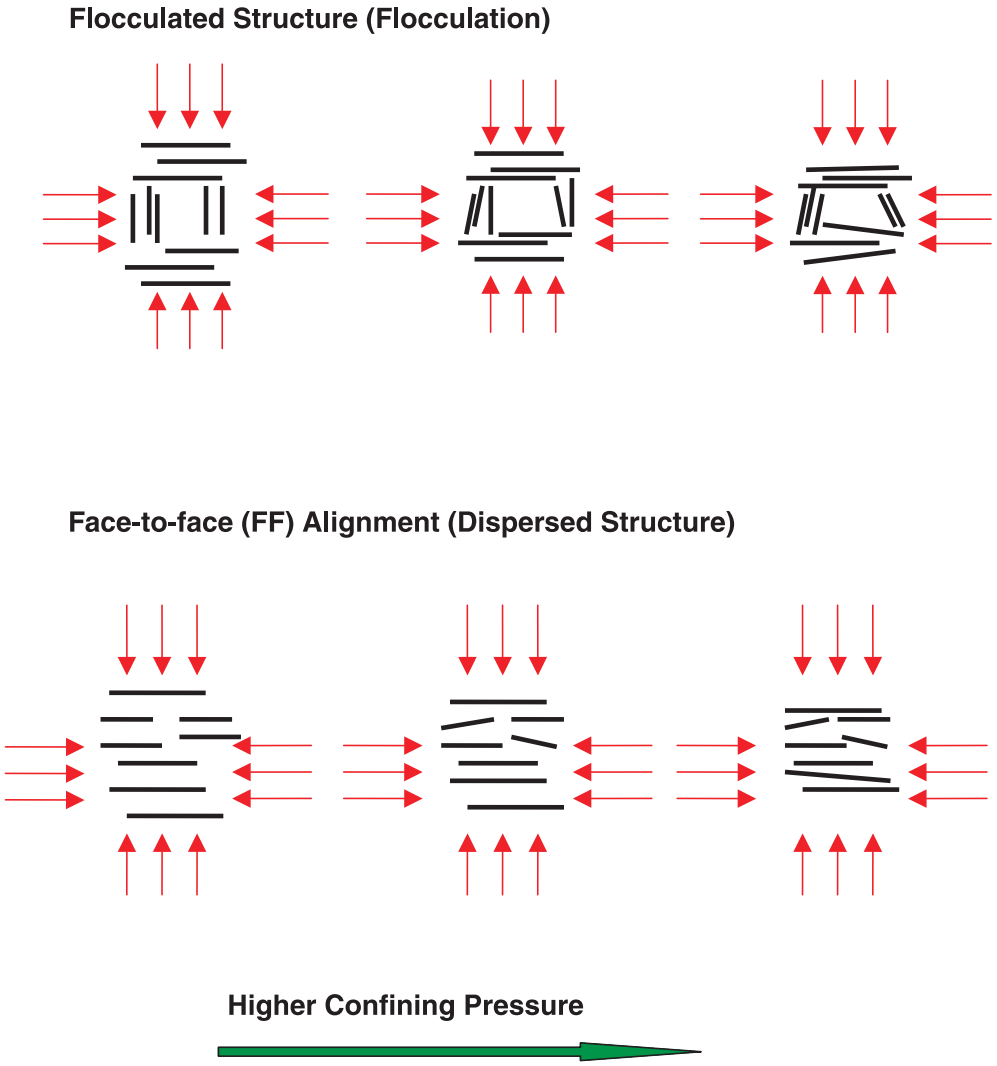

description) prevails at higher pH. Note that the packing of FF alignment exists in the (consolidated) sediment of the clay suspension with a dispersed and deflocculated structure.

The volume change can be attributed to particle orientation, rolling, and sliding and compression of the double layer (Sridharan and Venkatappa Rao 1973; Sridharan and Jayadeva 1982; Mitchell 1993). For the pH 7.8 specimen (a dispersed and deflocculated structure in the suspension), a closely packed FF alignment (in the sediment) can effectively reduce the extent of particle orientation and rolling, so the volume change can be considered mainly due to changing the double-layer thickness between particle faces. This is illustrated in Fig. 3. This deformation is limited because of strong double-layer repulsion. The larger inter-aggregate pores in the flocculated structure give more freedom for particle rearrangement, however, and thus the compressibility should be higher. This assertion agrees with the comment by Delage and Lefebvre (1983) to the effect that intermediate structure levels, which are not governed by double-layer phenomena, should be taken into account when considering the macroscopic compressibility behavior.

Further elaboration of the previous explanations can be discovered by examining the behavior of samples with added electrolytes (0.15 mol/L NaCl). Adding electrolytes decreases the degree of EF association at pH < IEP_{edge} but increases it at pH > IEP_{edge}. Therefore, the initial void ratio and compressibility of the pH 4 specimen decreased after adding electrolytes, whereas the pH 7.8 specimen performed in the opposite manner. In summary, soils with a higher degree of EF flocculation exhibit larger void ratios and higher compressibility in response to isotropic compression, which is in accordance with published trends (Mitchell 1993). Furthermore, the previous observations imply that the features of fabric association demonstrated at the deposition stage (i.e., the sediment) are preserved, to a certain extent, even under isotropic stresses up to 250 kPa. Even at this stress, the merging of these isotropic normal-consolidation lines is not readily seen.

Figure 2 also compares the compression behavior of specimens trimmed in the major ("vertical" specimen) and minor ("horizontal" specimen) principal directions. For the pH 7.8 sample, the initial void ratio of the horizontal specimen is

Fig. 4. The ratio of $\Delta\varepsilon_r/\Delta\varepsilon_a$ of specimens under different confining pressures.

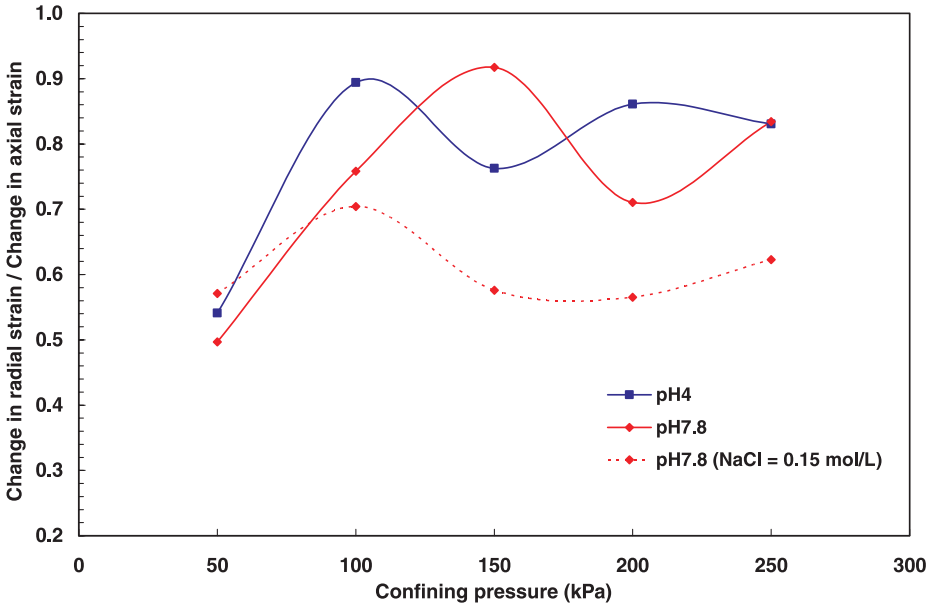

larger than that of the vertical specimen, although their pore-fluid properties are identical. For the two pH 4 specimens, the differences in the initial void ratio are not apparent because their main structure is EF associations, which are randomly arranged. In isotropic confinement above 100 kPa, specimens at the same pH trimmed in the two perpendicular directions have almost identical compression indices, as indicated in Table 2.

Strain response under isotropic confinement

The deformation behavior of soils can be better revealed by looking at the individual strain response in the axial and radial directions. Representative cases are shown in Fig. 4 in terms of the ratio between changes in the radial and axial strains (i.e., $\Delta\varepsilon_r/\Delta\varepsilon_a$), which are determined by the following equations:

$$[1] \qquad \Delta\varepsilon_{a,\,i+1} = (H_i - H_{i+1})/H_{\text{initial}}$$

$$[2] \qquad \Delta\varepsilon_{r,\,i+1} = (D_i - D_{i+1})/D_{\text{initial}}$$

where H and D are the height and diameter of the specimen, respectively. For instance, the ε_a indicated at the confinement of 100 kPa is calculated from the height difference between the present stage 100 kPa (H_{i+1}) and the previous stage 50 kPa (H_i). Note that the diameter is derived from the measured axial strain and the volume change.

As shown in Fig. 4, changes in axial strains were larger than the variations in radial strains. For the pH 7.8 specimen, this behavior (i.e., $\Delta\varepsilon_a > \Delta\varepsilon_r$) gives further evidence that changing the double-layer thickness governs the deformation of samples with the FF alignment. For the pH 4 specimen, such a strain anisotropic response can be attributed to different causes. Experimental observations and numerical simulations reveal that the clay particles tend to align along the major principal plane during 1D consolidation (Martin and Ladd 1978; Hicher et al. 2000; Yao and Anandarajah 2003). Hence, prestraining of the EF structure along the major principal direction is produced by the 1D consolidation during sample preparation. Such prestraining favors axial deformation even after the isotropic confinement is applied, so the ratio of strain changes is always less than one. Further evidence to support such explanations can be found by studying the behavior of the pH 7.8 specimen with the addition of electrolytes. The formation of flocculated structure of this specimen is mainly due to van der Waals attraction, and therefore its skeletal resistance is weaker than that of the pH 4 specimen where the fabric network is linked by Coulombian attraction. The influence of prestraining is therefore greater for the pH 7.8 sample with electrolytes, and an even lower ratio of strain changes can be found.

Resonant column test

Effects of pH on G_{max}

Figure 5 shows that the small-strain (or maximum) shear modulus, G_{max}, increases with a decrease in pH under the confinement ranging from 50 to 250 kPa. This trend, together with the changes in void ratio presented in Fig. 2, indicates behavior inconsistent with previously published observations (Hardin and Black 1968; Dobry and Vucetic 1987): G_{max} decreases with an increase in void ratio. The contradiction is due to the structure effect (i.e., interparticle electrical forces and associated fabric formation). The EF association is linked together by strong Coulombian attraction at low pH. Such a network structure strengthens the small-strain stiffness of the soil skeleton. At high pH, where double-layer repulsion prevails, the particle associations are weak and so is the associated stiffness. Note that the difference in G_{max} between pH 4 and pH 7.8 specimens increases with an increase in confining pressure. In other words, the influence of the structure is more pronounced under higher isotropic confinement.

Effects of pH on D_{min}

The small-strain (or minimum) damping ratio D_{min} decreases with a decrease in pH, as shown in Fig. 6. To en-

Fig. 5. The effects of pH on the small-strain shear modulus (G_{max}).

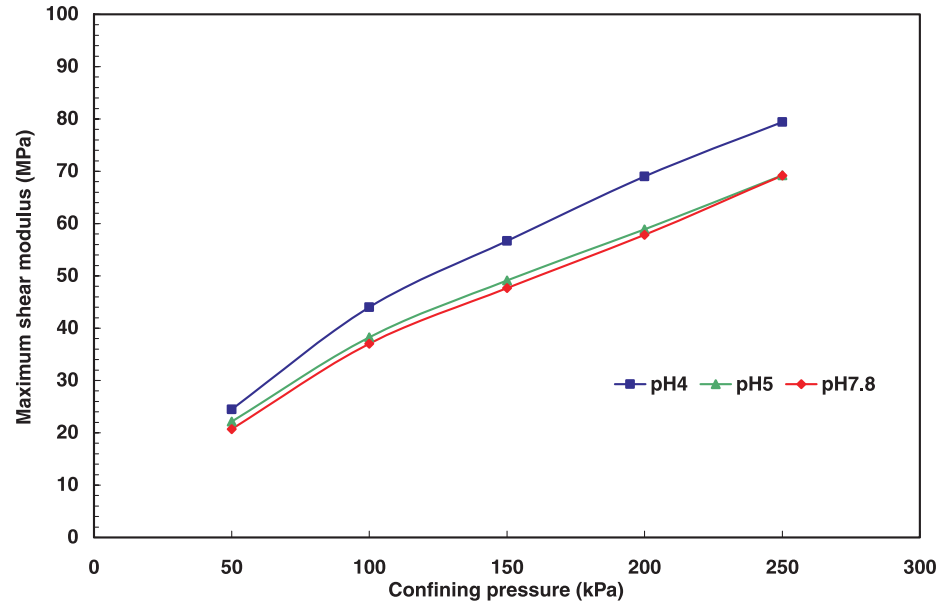

Fig. 6. The effects of pH on the small-strain damping ratio (D_{min}).

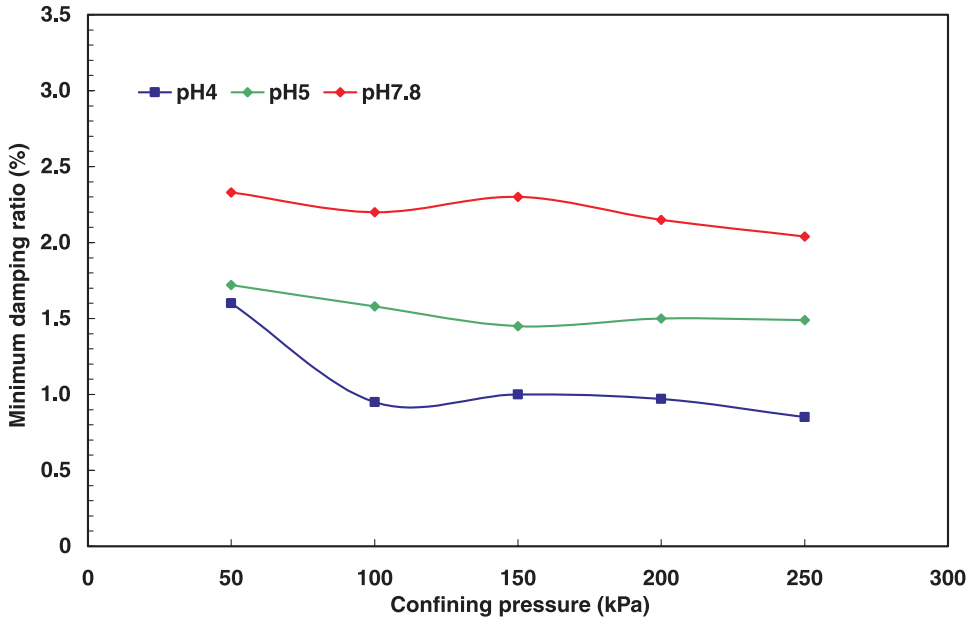

hance the understanding of these data, a short discussion of the attenuation mechanism related to local fluid motion is presented in the following.

It is generally accepted that the measured damping ratio of geomaterials is a lump sum result of two types of energy loss: viscous loss and frictional loss. At small strains, the damping ratio, D_{min}, is independent of strain, so the viscous loss prevails (Winkler et al. 1979). The higher viscous loss occurring in clays explains the published findings that the D_{min} of clays is much higher than that of sands, as pointed out by Lanzo and Vucetic (1999). The relevant energy-loss mechanisms accounting for this viscous loss in clays remain unclear, however. For saturated geomaterials, viscous losses associated with pore-fluid flow have been widely studied. It has been shown that the effect can be separated into macroscopic flow (i.e., Biot flow) and local flow (i.e., squirt flow) (Mavko et al. 1979; Bourbié et al. 1987). For materials with low permeability and skeletal stiffness, such as clays, the loss related to Biot flow becomes irrelevant (Santamarina et al. 2001). In this context, the energy loss due to local fluid motion between pores and around contacting grains gains significance. Such a loss mechanism might then account for the high D_{min} values of clays. Indeed, this type of energy loss has been used to explain the damping ratio of saturated sands (Bolton and Wilson 1990; Cascante et al. 1998; Ellis et al. 2000).

Bolton and Wilson (1990) derived the damping ratio D_v associated with local fluid motion:

Fig. 7. Illustrations of energy loss related to local fluid motion for soils with different structures.

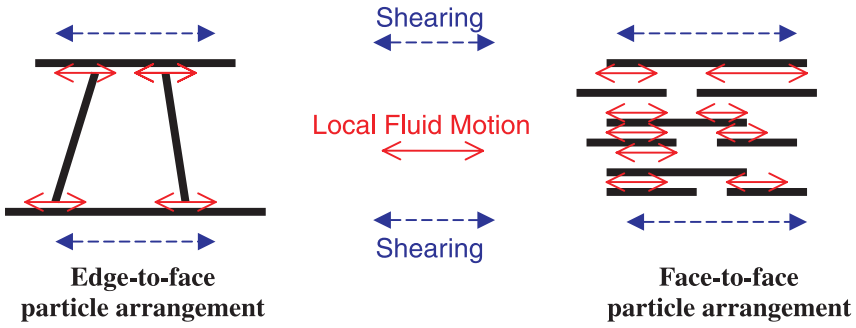

Fig. 8. The effects of ionic strength on the small-strain shear modulus (G_{max}).

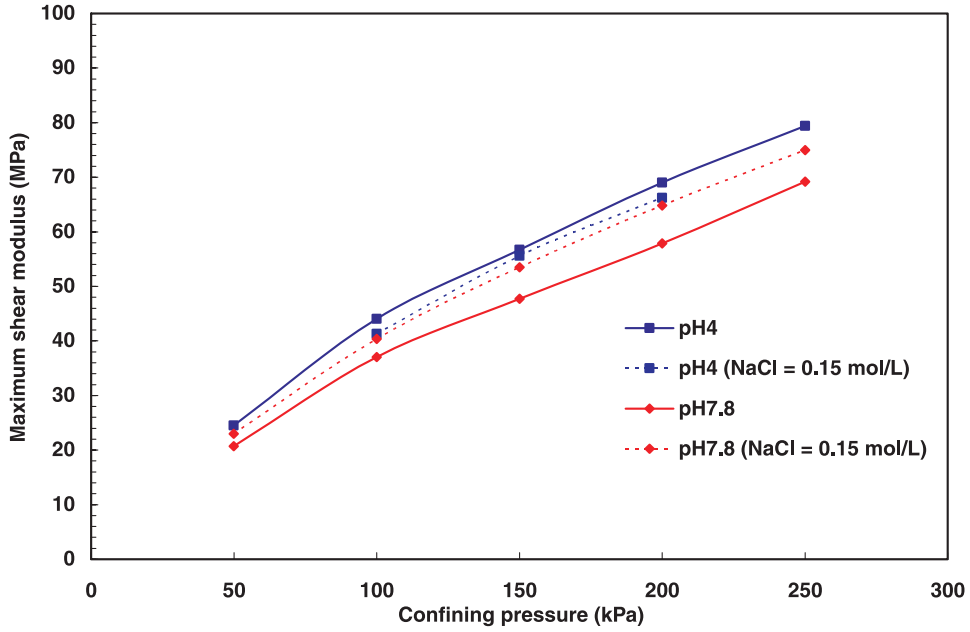

$$[3] \qquad D_v \propto \frac{F_v \mu f}{G}$$

where μ is the pore fluid viscosity, f is the frequency, G is the shear modulus of the soil skeleton, and F_v is a dimensionless fluid dissipation factor related to the soil microstructure and micromechanics. Ellis et al. (2000) extended this expression, concentrating on this phenomenon at particle contacts and considering the strain effects. Their version of eq. [3] is as follows:

$$[4] \qquad D_v \propto \frac{\mu f}{G}(M)^{1/3}$$

where M is the particle contact per unit volume where the local fluid motion is generated. The parameter M is a function of strain. This expression by Ellis et al. implies that a soil with more intergranular contacts, such as a soil with a larger proportion of small particles, will have a higher damping ratio. Also, higher skeletal stiffness G can lead to a lower damping ratio (note that the damping ratio is a ratio between the lost and the stored energy). Although the soil type in these two studies was saturated sand, the studies can still provide a general idea about the factors influencing such losses in clays. If the fabric arrangement favors local fluid motion (e.g., more contacts) or the soil has a lower skeletal stiffness, a higher damping ratio D_{min} is expected.

Following this reasoning, the trend shown in Fig. 6 of D_{min} decreasing with a decrease in pH is not only because the low-pH specimen has a higher G_{max}, but also because of the associated energy-loss mechanisms. Note that the difference in damping ratio between the pH 4 and pH 7.8 specimens is much greater than the differences seen in the shear modulus. As explained previously, the D_{min} value can be considered primarily due to the viscous loss related to pore-fluid motion around particle contacts. Therefore, as illustrated in Fig. 7, soil with a flocculated structure (such as the pH 4 specimen), due to its open packing, has fewer particle contacts where fluid motion in response to particle shearing can take place. The result is a smaller damping ratio.

Effects of ionic strength on G_{max} *and* D_{min}

The addition of NaCl electrolytes promotes the formation of flocculated structure in samples with pH > IEP_{edge} because van der Waals attraction prevails. On the other hand, this action will weaken the EF association at pH < IEP_{edge} because of the reduction in the mutual Coulombian attraction between the positive edge and the negative face. The

Fig. 9. The effects of ionic strength on the small-strain damping ratio (D_{min}).

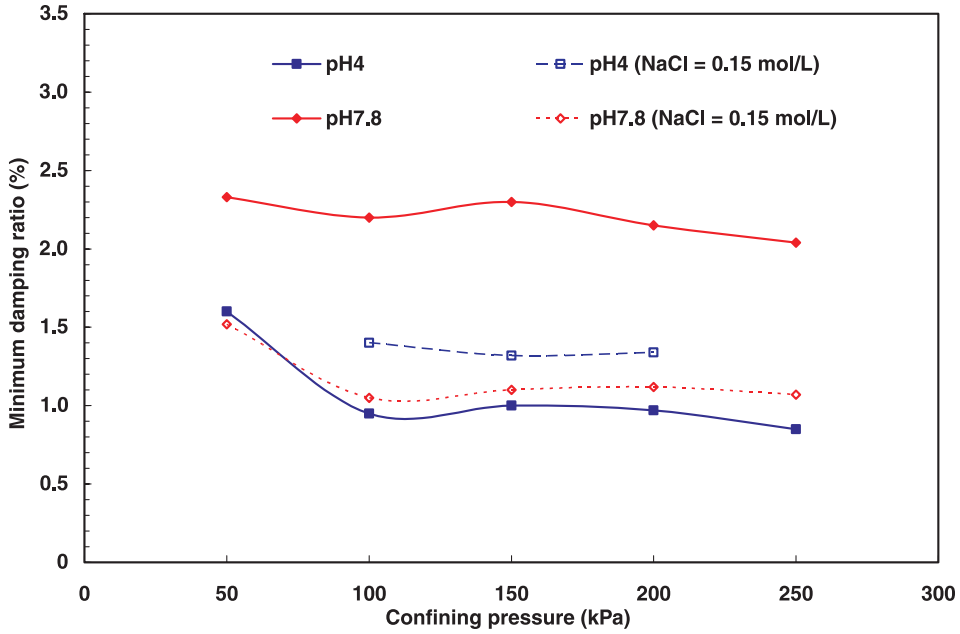

Fig. 10. The effects of fabric anisotropy on the small-strain shear modulus (G_{max}).

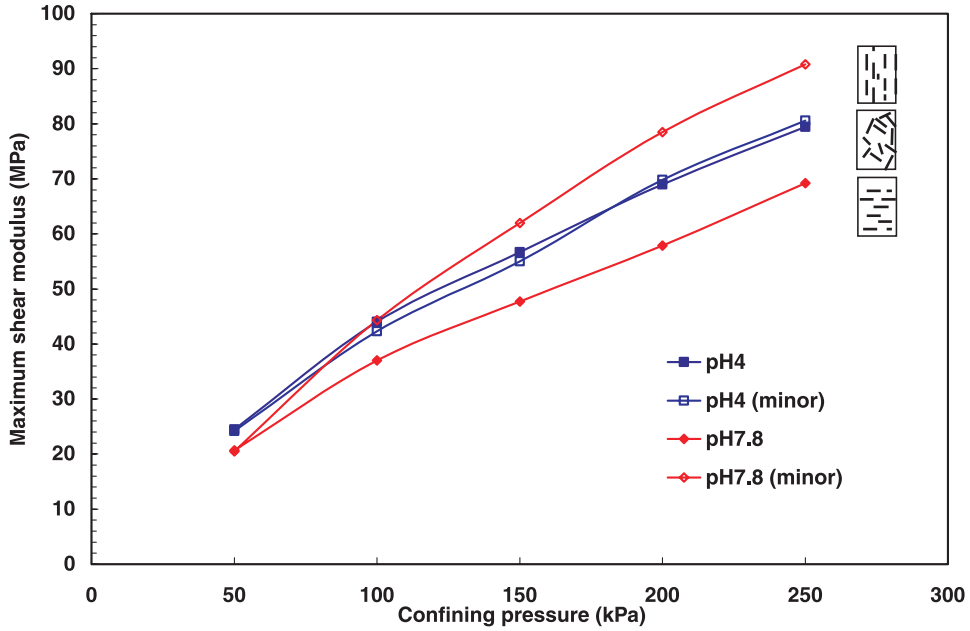

linkup of soil skeletons depends on these attractive forces, and the measured G_{max} is expected to follow a similar trend. As shown in Fig. 8, the G_{max} of the pH 4 specimen decreases after adding electrolytes, and the pH 7.8 specimen shows the opposite behavior. The value of G_{max} increases with an increase in the degree of flocculation and stronger interparticle attractive forces. Moreover, the behavior of the modulus for the pH 4 specimens with and without electrolytes explains the contradiction mentioned in Table 1: the *S*-wave velocity of kaolinite specimen deceases with an increase in ionic strength (Santamarina and Fam 1995).

The D_{min} of pH 7.8 specimens decreases after adding electrolytes, whereas the pH 4 specimens behave in the opposite fashion (Fig. 9), i.e., D_{min} decreases with an increase in the degree of flocculation. The explanation is probably similar: increasing the degree of flocculation increases the skeletal stiffness and decreases the number of particle contacts to facilitate fluid motion. Both factors tend to result in a lower damping ratio.

Effects of fabric anisotropy on G_{max} *and* D_{min}

Since resonant column testing can only reveal the overall shear modulus and damping ratio of soils, the effects of inherent fabric anisotropy were investigated using an alterna-

Fig. 11. The effects of fabric anisotropy on the small-strain damping ratio (D_{min}).

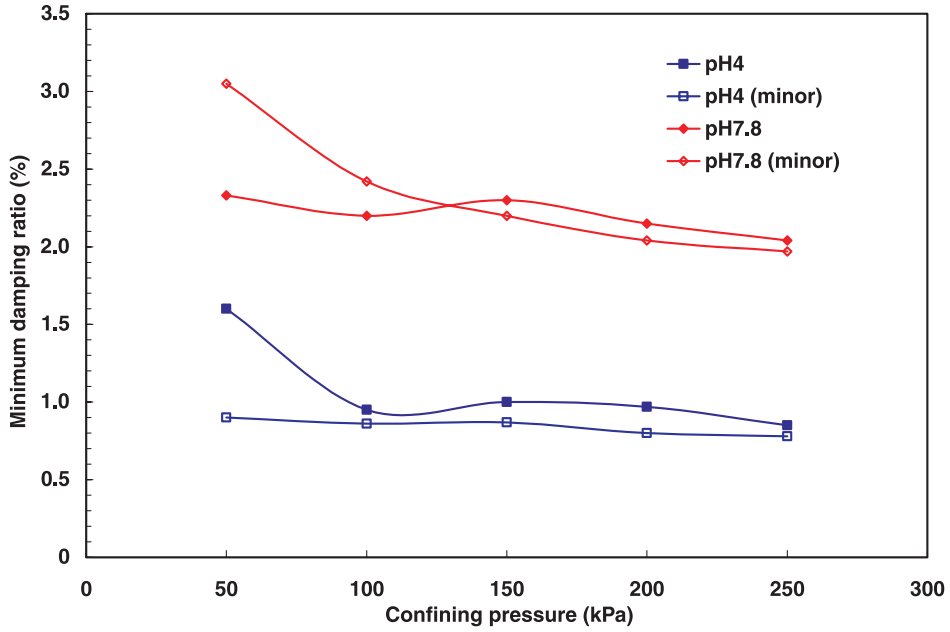

Fig. 12. Illustrations of particle movement with respect to shearing for the vertical and horizontal pH 7.8 specimens.

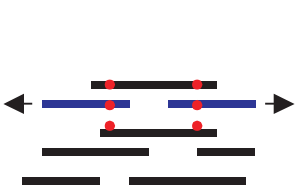

Particle orientation is parallel to the direction of particle motion

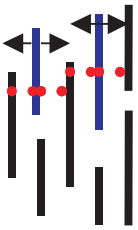

Particle orientation is perpendicular to the direction of particle motion

tive method, namely testing the pH 4 and pH 7.8 samples trimmed in two perpendicular directions. The results are shown in Figs. 10 and 11.

At pH 7.8, the G_{max} value of the horizontal specimen was greater than that of the vertical specimen (Fig. 10), even though it possessed a higher void ratio (as can be seen in Fig. 2). Such behavior can be explained by looking into the details of the reacting interparticle forces in response to small-strain shearing. As illustrated in Fig. 12, particle movement in the vertical sample is mainly hindered by van der Waals attraction. On the other hand, for the horizontal specimen, the movement is mainly resisted by double-layer repulsion. With increasing confinement, the separation distance between particles is reduced, so a larger double-layer repulsion and (or) even stronger short-range repulsion such as Born repulsion and solvation (hydration) forces come into play. As a result, the G_{max} difference between the two pH 7.8 specimens increases with an increase in confinement, and the G_{max} of the pH 7.8 horizontal specimen becomes greater than that of the pH 4 specimens, which had stronger interparticle forces and an EF network.

There is no difference in D_{min} between the two pH 7.8 specimens, except at the transition of stress states from the K_0 condition to isotropic confinement ($\sigma'_0 < 100$ kPa), as shown in Fig. 11. The ratio of D_{min} between the vertical and horizontal specimens at 250 kPa confinement is 1.04. Comparing only the energy-loss portion, however, the ratio was higher at 1.36. This is because the vertical specimen had a smaller modulus and therefore lower stored energy influencing the damping ratio. This observation suggests that particle movement in the horizontal specimens facilitates pore fluid movement to increase the energy loss and the associated damping ratio.

The results for the two pH 4 specimens, as expected, showed similar G_{max} values, suggesting the insignificance of stiffness anisotropy due to inherent fabric arrangement. Indeed, the flocculated structure exhibited random particle orientation. Moreover, the D_{min} values of these two specimens were also similar except at the transition of stress states ($\sigma'_0 < 100$ kPa).

Effects of confining pressure on G_{max} *and* D_{min}

The shear modulus G_{max}, as expected, always increases with an increase in confining pressure, but the increment is dependent on the soil structure. The modulus–stress relationship is used for further discussions on this matter:

Fig. 13. The logarithm–logarithm plot of modulus versus confinement.

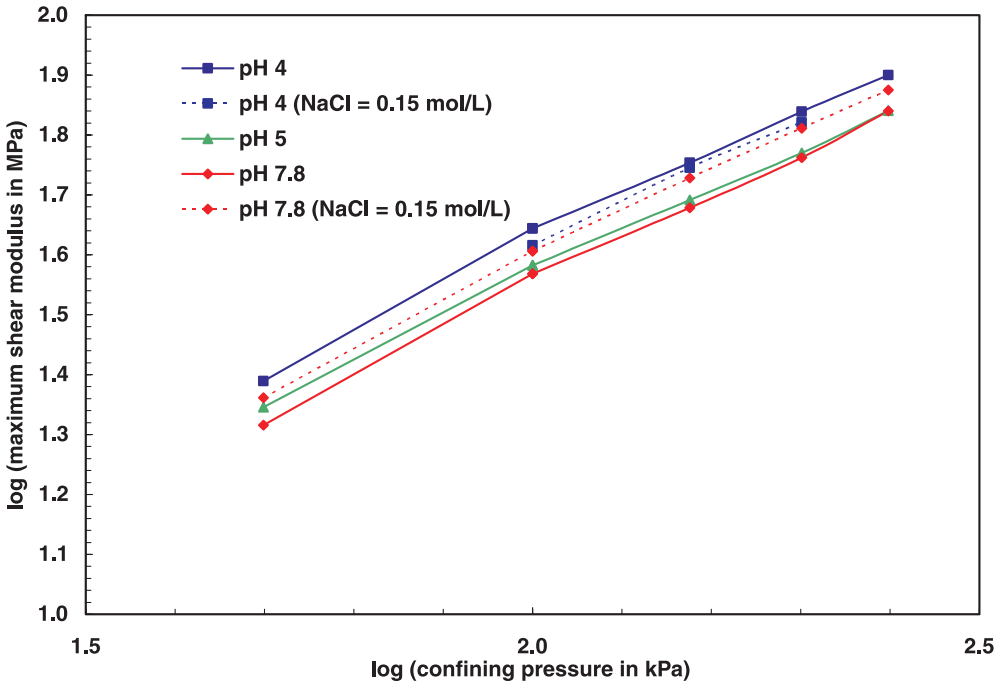

Table 3. The α and β parameters of the modulus–stress relationships for soils with different structures under isotropic confinement.

	α (MPa)		β	
Pore fluid properties of soil sample	$\sigma'_0 \leq 100$ kPa	$\sigma'_0 \geq 100$ kPa	$\sigma'_0 \leq 100$ kPa	$\sigma'_0 \geq 100$ kPa
pH 4	0.895	2.24	0.846	0.647
pH 4 and [NaCl] = 0.15 mol/L	—	1.78	—	0.684
pH 5	1.020	1.97	0.786	0.643
pH 7.8	0.778	1.62	0.839	0.677
pH 7.8 and [NaCl] = 0.15 mol/L	0.957	1.81	0.813	0.676

$$[5] \qquad G_{max} = \alpha \left(\frac{\sigma'_0}{1 \text{ kPa}} \right)^{\beta}$$

where G_{max} is the shear modulus, α and β are fitting parameters, and σ'_0 is the isotropic confining pressure. The variations of G_{max} in response to different confining pressures are shown in Fig. 13 in a logarithm–logarithm plot; the fitting parameters α and β are listed in Table 3. Note the boundary separating the two different modulus–stress relationships at the confinement of 100 kPa. The stiffness response to isotropic loading apparently becomes stable at confinements greater than 100 kPa.

The α and β parameters can capture the features of contact behavior in response to the state of stress (Santamarina et al. 2001). Collectively speaking, a higher α value represents a soil that has a stronger packing or stiffer particles; a higher β value indicates that the soil stiffness is more sensitive to confinement (reflecting relatively weaker interparticle forces) and (or) has greater compressibility (reflecting relatively more severe fabric changes due to loading). Comparing the same specimen below and above the 100 kPa confinement, a higher β value is observed for lower confinements. This indicates greater fabric changes due to altering the stress state. Supporting evidence for this is found in Fig. 14, where the change in volumetric strain in response to the confining pressure is presented. The greatest volumetric changes occurred as the confinement increased from 50 to 100 kPa. At $\sigma'_0 \geq 100$ kPa, soil specimens with stronger flocculated structures exhibited slightly higher α values and lower β values, and soil specimens with weak dispersed structures showed slightly lower α values and higher β values. This is in accordance with the previous discussions.

The influence of confinement on the small-strain damping ratio D_{min} can be seen in Figs. 6, 9, and 11. D_{min} decreases when the confining pressure increases from 50 to 100 kPa and then becomes nearly constant at higher confining pressures. In other words, except for the transition stage of changing the stress state, D_{min} is independent of the isotropic confinement.

Normalized modulus (G/G_{max}) and damping ratio (D/D_{min}) curves

Figures 15 and 16 present the normalized modulus (G/G_{max}) and damping ratio (D/D_{min}) curves, respectively, of soils with different structures under an effective confinement

Fig. 14. Changes in volumetric strains, $\Delta\varepsilon_v$, under different confining pressures. The value of $\Delta\varepsilon_v$ is calculated based on eqs. [1] and [2], i.e., $\Delta\varepsilon_v = \Delta\varepsilon_a + 2\Delta\varepsilon_r$.

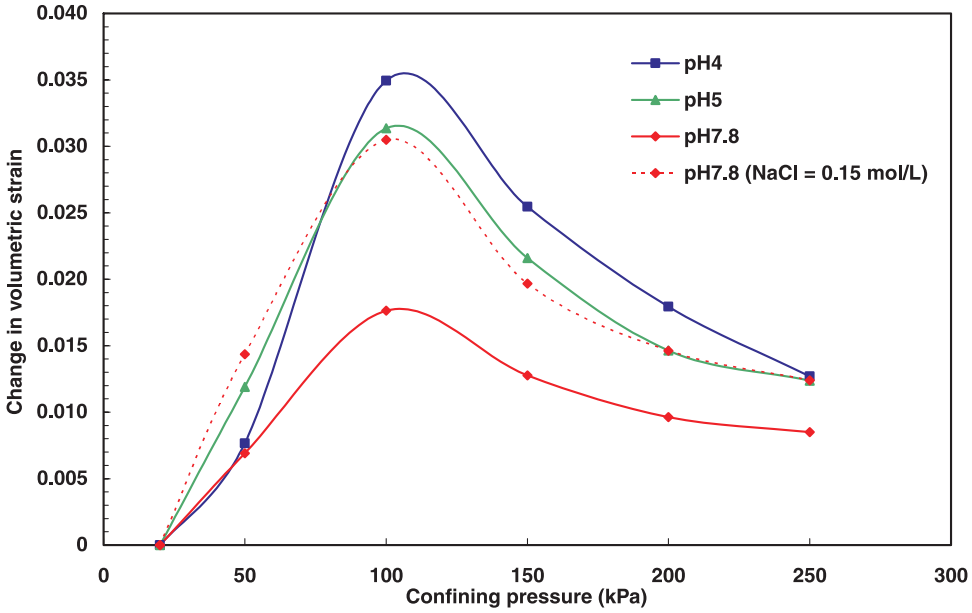

Fig. 15. The normalized modulus curve (G/G_{max}) under an effective confinement of 250 kPa for soils with different structures. The broken lines represent the empirical relations proposed by Vucetic and Dobry (1991).

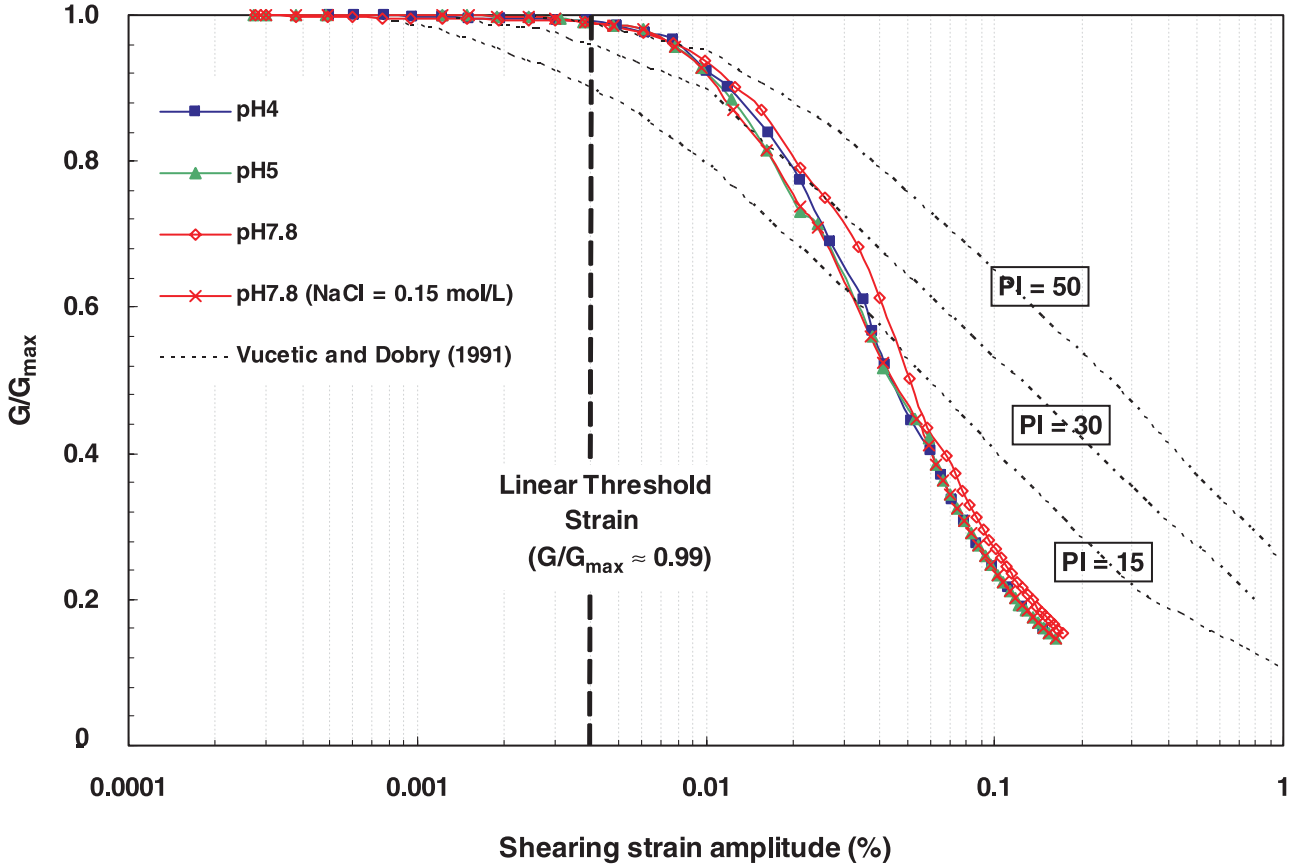

of 250 kPa. The empirical relations related to the plasticity index (PI) proposed by Vucetic and Dobry (1991) are also shown. Although the plasticity index PI of kaolinite samples with different structures ranges from 16 to 30, the normalized modulus and damping ratio curves are very similar. The observed PI independence may be due to higher confine-

Fig. 16. The normalized damping ratio curve (D/D_{min}) under an effective confinement of 250 kPa for soils with different structures. The broken lines represent the empirical relations proposed by Vucetic and Dobry (1991) for which the y-axis is damping ratio in percentage instead.

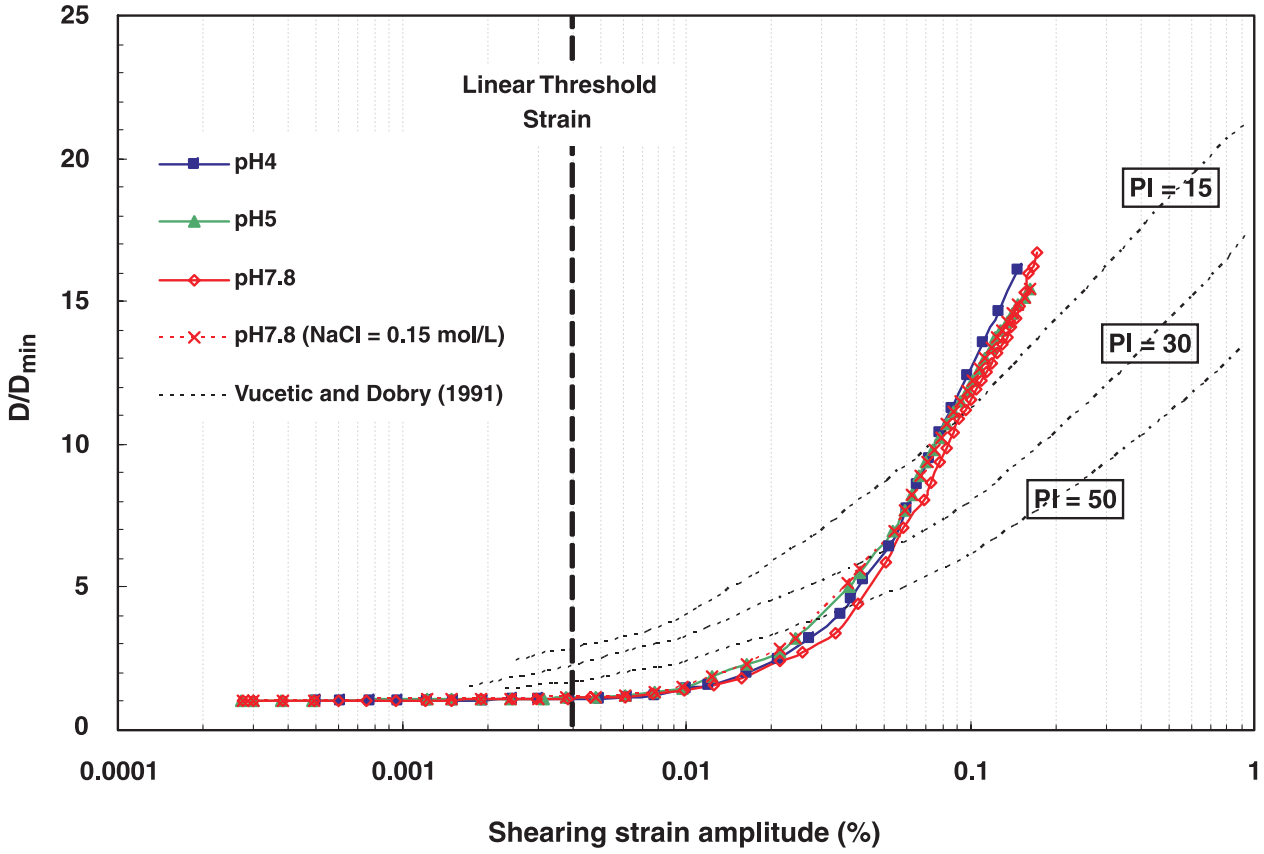

Fig. 17. Effective stress paths of pH 4 and pH 7.8 specimens (where e_0 is the initial void ratio).

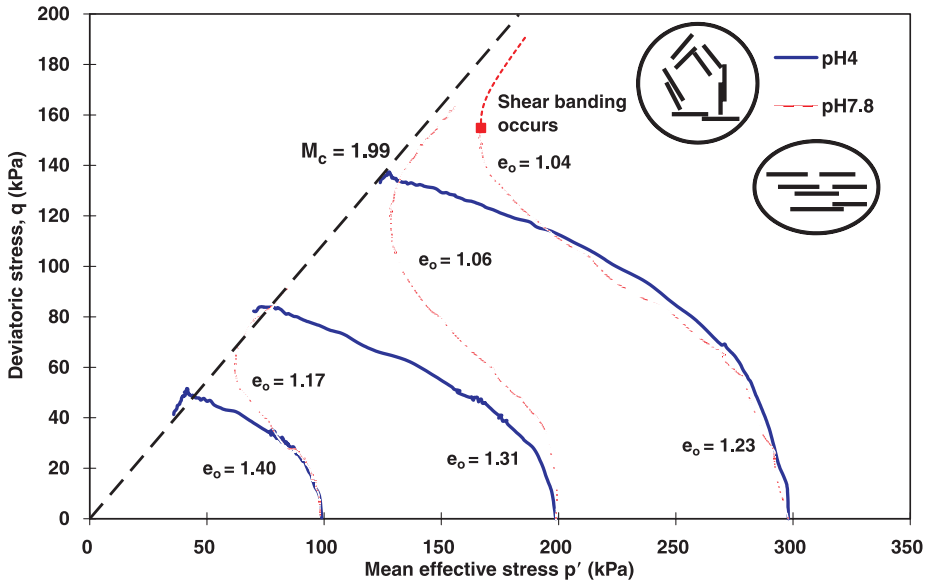

ment. As indicated in the empirical relations suggested by Ishibashi and Zhang (1993), the dependence on PI decreases with an increase in confinement.

The linear threshold strain was approximately 0.004%, which is greater than would be predicted by the empirical relations for the case where PI = 30 (Vucetic and Dobry

Fig. 18. Effective stress paths of specimens at the effective confinement 100 kPa (where e_0 is the initial void ratio).

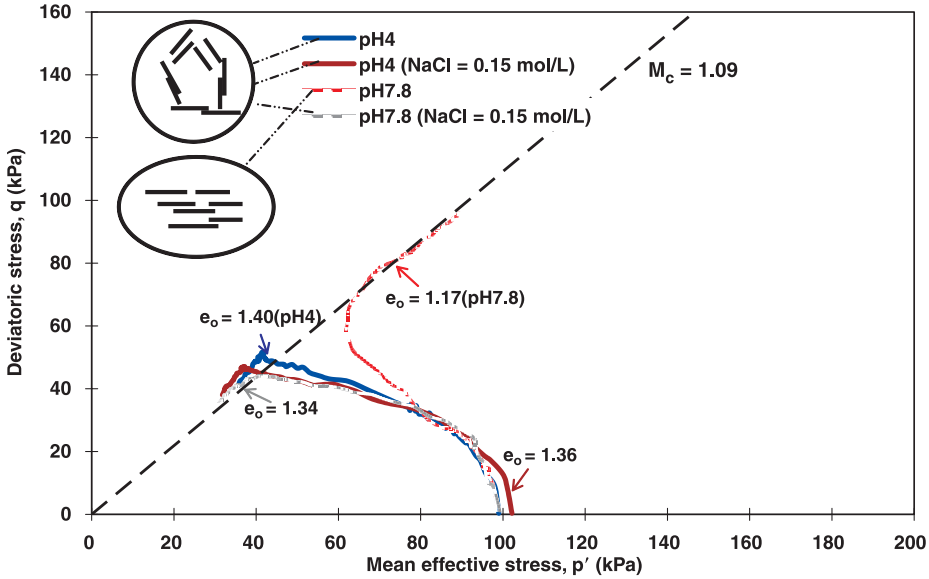

1991). Furthermore, after the curves depart from the constant plateau with respect to the strain, the variation is greater than the that indicated by the empirical relations.

Triaxial test

Effects of pH on the stress–strain behavior and undrained shear strength S_u

Figure 17 presents effective stress paths of specimens at pH 4 and pH 7.8 under three different confining pressures. The pH 4 specimens exhibit contractive tendencies towards the critical state. A critical-state line for the triaxial compression tests with a slope M_c = 1.09 can be obtained; the corresponding critical-state friction angle ϕ'_c is 27.5°. The pH 7.8 specimens demonstrated completely different responses: they contracted initially, passed through a phase-transformation state, and then dilated with the same stress ratio. Although the pH 7.8 specimens did not behave the same as the pH 4 specimens, which always reached a well-defined critical state within a tolerable strain range of ~25% (the specimen deformed too much for accurate measurements at larger strains), the trends still suggest that the critical stress ratio of the pH 7.8 specimen was close to that of the pH 4 specimens. The dilative response of the pH 7.8 specimens may be attributed to the closely packed fabric and strong double-layer repulsive forces. It is interesting to observe the phase transformation behavior, which generally occurs in sand.

Table 4 lists the measured undrained shear strength S_u at the ultimate state. For the pH 4 specimens, the value was much lower than that for the pH 7.8 specimens at all confinements, although the interparticle attraction in pH 4 specimens is stronger. In contrast with the stiffness behavior and previously published results (Moore and Mitchell 1974; Sridharan and Prakash 1999; Anandarajah and Zhao 2000), the interparticle attractive forces did not appear to have a strong influence on the undrained shear strength S_u for specimens under effective confinements greater than 100 kPa. On the contrary, the initial packing density, i.e., denser or looser, was the dominant factor in determining S_u, which is the same as typical soil behavior.

Table 4. Undrained shear strength (S_u) of soils with different structures at different confining pressures.

	S_u (kPa)	
Confining pressure (kPa)	pH 4 specimen	pH 7.8 specimen
100	19.5	48.1
200	40.3	79.0
300	66.0	77.5[a]

[a]The undrained shear strength S_u is expected to be larger than the measured value because the test was stopped at the onset of shear banding.

Effects of ionic strength on the stress–strain behavior

Figure 18 shows the effective stress path in the q–p' space of the specimens with electrolytes under an effective confinement of 100 kPa (where q is the deviatoric stress, and p' is the mean effective stress). The specimens without excess electrolytes are also shown for comparison. The specimens at pH 4 and pH 7.8 with 0.15 mol/L NaCl exhibited behavior similar to that of the pH 4 specimens without excess electrolyte, namely showing a contractive tendency towards the critical state. This reveals that soils behave similarly in response to shearing if they all have a flocculated structure. Moreover, specimens with electrolytes attain the same critical stress ratio as that of the pH 4 specimens, suggesting that the critical-state line in the q–p' plane is independent of interparticle forces and the initial soil fabric. This behavior supports the conceptual model proposed by Lambe (1960), which is that the shear strength is mainly controlled by particle friction at large strains. Also, this friction behavior is in accordance with the microscopic model proposed by Matsui et al. (1980). The friction angle ϕ' (and the slope of the M_c line) depends mainly on the mineral type. In summary, for the kaolinite clay used in this study, the critical-state stress

Fig. 19. The deformation characteristics of specimens in the e – lnp' plane.

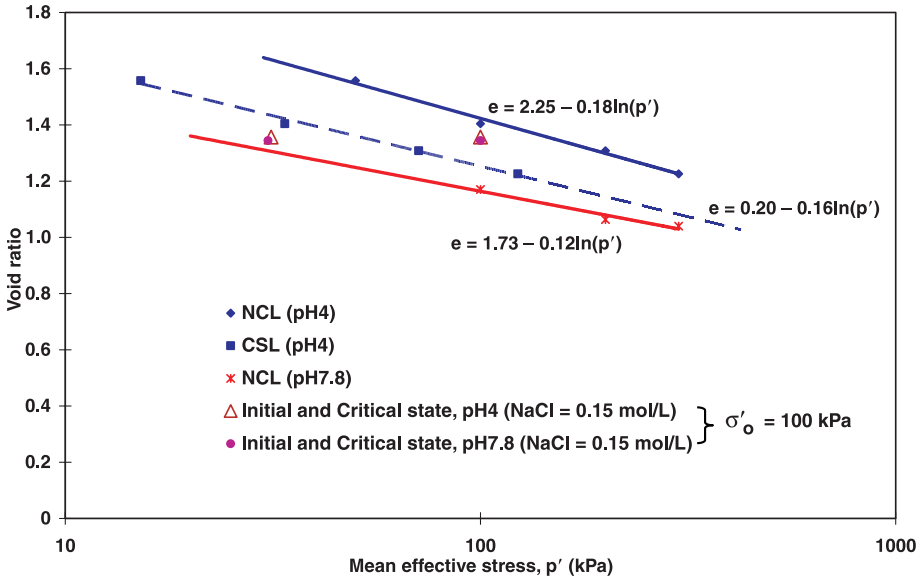

ratio for the compression test is similar regardless of the interparticle forces and associated fabrics.

Normal consolidation line and critical-state line in e – *ln*p′ *space*

The soil response at the critical state in void ratio (e) – lnp' space is shown in Fig. 19. As noted previously, soils with different fabric associations apparently render individual normal consolidation lines (NCL) and different volumetric responses. Hence, two different normal consolidation lines can be found for soils with flocculated associations (pH 4) and dispersed structures (pH 7.8, FF alignment). The critical-state line (CSL) of the pH 4 specimens in the e – lnp' space is also shown in Fig. 19. It can be seen that the NCL of the pH 4 specimen is steeper than its CSL (not parallel), which implies that normally consolidated samples show stronger contraction tendencies (or higher excess positive pore-water pressure) under lower effective confining pressures when subjected to undrained shearing.

The initial and critical states of the pH 4 and pH 7.8 specimens with electrolytes in the e – lnp' plane are also indicated in Fig. 19 (under an effective confinement of 100 kPa). The initial and critical states of these two specimens do not lie on the NCL and CSL of the pH 4 specimen. That is, the soil structure affects not only the normal consolidation response, but also the critical state in the e – lnp' plane. This behavior is similar to that observed by Wheeler and Sivakumar (2000): the macrofabric (inter-aggregate pores) is sheared to the critical state, but the microfabric of individual clay packets (intra-aggregate pores) may not reach a state such that the influence of the initial fabric is not completely erased. Also, these discussions implicitly echo the comments made by Kuganenthira et al. (1996): the anisotropy effects on the stress–strain behavior are controlled by cluster-to-cluster orientation rather than particle-to-particle orientation. Nevertheless, further study is required to verify the non-uniqueness of the CSL in e – lnp' space and the associated causes.

Conclusions

The Speswhite Kaolin with known and controlled fabric associations was used to investigate the effects of structure on the mechanical responses of the material. The initial void ratio of the soil packing and its compressibility were found to be intimately related to the soil structure. Individual normal consolidation lines can be discovered for soils with different structures, and any merging trend is not readily seen for isotropic confinements up to 250 kPa. When the EF association dominates, the samples possess larger void ratios and higher compressibility, which is associated with the inter-aggregate pores. On the other hand, denser specimens with lower compressibility due to stronger double-layer repulsion are observed when the FF alignment prevails. The strain response never becomes isotropic, even when subjected to higher confinements. Such anisotropic behavior, with the axial strain always greater than the radial strain, is because of the inherent fabric anisotropy formed at the deposition stage and (or) the prestraining effects occurring during K_0 consolidation in the sample preparation.

The influence of structure on the dynamic properties at small strains (i.e., G_{max} and D_{min}) is apparent. The EF association, linked by strong Coulombian attraction at pH < IEP_{edge}, demonstrates a higher G_{max}. At pH > IEP_{edge}, where double-layer repulsion prevails, the linkup is weakened and so is the associated G_{max}. The addition of NaCl electrolytes promotes the formation of a flocculated structure in specimens with pH > IEP_{edge} because van der Waals attraction prevails. This weakens the EF association at pH < IEP_{edge} by reducing Coulombian attraction between the positive edge and the negative face. Although the linkup of soil skeletons depends on these attractive forces, the magnitude of G_{max} follows the degree of flocculation. D_{min} is associated with the energy loss related to the local fluid motion and the skeletal stiffness G_{max}. Soils with a flocculated structure possess higher G_{max} and have fewer particle contacts, which facilitates fluid motion in response to shearing. As a result, a

smaller damping ratio is observed. On the other hand, soils with the face-to-face alignment such as that of the pH 7.8 specimen exhibit the opposite characteristics and therefore have a higher damping ratio. It should be noted that the damping ratios D_{min} of soils with different structures demonstrate confinement independence.

The horizontal and vertical specimens at pH 7.8 show very different G_{max} values because of the different particle alignment and the reacting interparticle forces in response to shearing. Because the particle arrangement in the EF network is random, the two pH 4 specimens (horizontal and vertical) show similar G_{max} values. Although the plasticity index PI of kaolinite specimens with different structures ranges from 16 to 30, the normalized modulus and damping ratio curves are very similar. Such PI independence may be due to the higher confinement applied (250 kPa). The linear threshold strain was similar for all specimens, about 0.004%, but greater than that predicted by the empirical relations of Vucetic and Dobry (1991).

Interparticle attractive forces do not have an apparent influence on the shear strength at the critical state. The critical-state line in the q–p' plane obtained from undrained triaxial compression tests seems unrelated to the pore-fluid properties and the associated initial soil structure. The slope M_c was found to be 1.09, and the corresponding critical-state friction angle was 27.5°. The undrained shear strength S_u was also unrelated to the interparticle attractive forces, and, similar to typical soil behavior, the initial packing density is the dominant factor determining S_u.

The soil structure affected the stress–strain behavior. Specimens with a flocculated structure exhibit a contractive tendency until reaching the critical state, whereas specimens with the FF alignment demonstrated more complicated behavior as follows: contracting initially, passing through a phase transformation state, and then dilating with the same stress ratio. In the $e - \ln p'$ plane, the soil structure not only produced unique normal consolidation lines, but also resulted in different critical states for specimens under the same confinement (100 kPa).

Acknowledgements

This research was supported by the Research Grants Council (grant HKUST6034/02E), Hong Kong, and the Hong Kong University of Science and Technology (HIA04/05.EG02). The authors are grateful to reviewers for valuable comments.

References

Anandarajah, A., and Zhao, D. 2000. Triaxial behavior of kaolinite in different pore fluids. Journal of Geotechnical and Geoenvironmental Engineering, ASCE, **126**(2): 148–156.

Anandarajah, A., Kuganenthira, N., and Zhao, D. 1996. Variation of fabric anisotropy of kaolinite in triaxial loading. Journal of Geotechnical Engineering, ASCE, **122**(8): 633–640.

Bolton, M.D., and Wilson, J.N. 1990. Soil stiffness and damping. *In* Structural dynamics. *Edited by* W.B. Krazig. A.A. Balkema, Rotterdam, The Netherlands. pp. 209–216.

Bourbié, T., Coussy, O., and Zinszner, B. 1987. Acoustics of porous media. Gulf Publishing Co., Houston, Tex.

Cascante, G., Santamarina, C., and Yassir, N. 1998. Flexural excitation in a standard torsional-resonant column device. Canadian Geotechnical Journal, **35**(3): 478–490.

Delage, P., and Lefebvre, G. 1983. Discussion on double layer theory and compressibility of clays. Géotechnique, **33**(2): 461.

Dobry, R., and Vucetic, M. 1987. State-of-the-art report: dynamic properties and seismic response of soft clay deposits. *In* Proceedings of the International Symposium on Geotechnical Engineering of Soft Soils, Mexico City, 13–14 August 1987. Sociedad Mexicana de Mecanica de Suelos AC, Mexico City. Vol. 2, pp. 51–87.

Du, B.L., Mikroudis, G.K., and Fang, H.Y. 1986. Effect of pore fluid pH on the dynamic shear modulus of clay. *In* Hazardous and industrial solid waste testing and disposal. *Edited by* D. Lorenzen, R.A. Conway, L.P. Jackson, A. Hamza, C.L. Perket, and W.J. Lacy. American Society for Testing and Materials (ASTM), Special Technical Publication STP 933, Vol. 6, pp. 226–239.

Edil, T.B., and Luh, G.F. 1980. Microstructural effects on dynamic response of clays. *In* Proceedings of the 7th World Conference on Earthquake Engineering, Istanbul, Turkey, 8–13 September 1980. *Edited by* Oktay Ergünay and Mustafa Erdik. Turkish National Committee on Earthquake Engineering, Ankara, Turkey. Vol. 3, pp. 133–140.

Ellis, E.A., Soga, K., Bransby, M.F., and Sato, M. 2000. Resonant column testing of sands with different viscosity pore fluids. Journal of Geotechnical and Geoenvironmental Engineering, ASCE, **126**(1): 10–17.

Hardin, B.O., and Black, W.L. 1968. Vibration modulus of normally consolidated clay. Journal of the Soil Mechanics and Foundations Division, ASCE, **94**(2): 353–369.

Head, K.H. 1994. Manual of soil laboratory testing. 2nd ed. Vol. 2. Halsted Press, John Wiley & Sons Inc., New York.

Hicher, P.Y., Wahyudi, H., and Tessier, D. 2000. Microstructural analysis of inherent and induced anisotropy in clay. Mechanics of Cohesive–Frictional Materials, **5**: 341–371.

Ishibashi, I., and Zhang, X. 1993. Unified dynamic shear moduli and damping ratios of sand and clay. Soils and Foundations, **33**(1): 182–191.

Kuganenthira, N., Zhao, D., and Anandarajah, A. 1996. Measurement of fabric anisotropy in triaxial shearing. Géotechnique, **46**(4): 657–670.

Lambe, T.W. 1960. A mechanistic picture of shear strength in clay. *In* Proceedings of the ASCE Conference on Shear Strength of Cohesive Soils, Boulder, Colo., June 1960. American Society of Civil Engineers (ASCE), New York, pp. 555–580.

Lanzo, G., and Vucetic, M. 1999. Effect of soil plasticity on damping ratio at small cyclic strains. Soils and Foundations, **39**(4): 131–141.

Li, X.S., Chan, C.K., and Shen, C.K. 1988. An automatic triaxial testing system. *In* Advanced triaxial testing of soil and rock. *Edited by* R.T. Donoghe, R.C. Chaney, and M.L. Silver. American Society for Testing and Materials (ASTM), Special Technical Publication STP 977, pp. 95–106.

Li, X.S., Yang, W.L., Shen, C.K., and Wang, W.C. 1998. Energy-injecting virtual mass resonant column system. Journal of Geotechnical and Geoenvironmental Engineering, ASCE, **124**(5): 428–438.

Martin, R.T., and Ladd, C.C. 1978. Fabric of consolidated kaolinite. Clays and Clay Minerals, **23**: 17–25.

Matsui, T.M., Ito, T., Mitchell, J.K., and Abe, N. 1980. Microscopic study of shear mechanisms in soils. Journal of Geotechnical Engineering, ASCE, **106**(GT2): 137–152.

Mavko, G., Kjartansson, E., and Winkler, K. 1979. Seismic wave attenuation in rocks. Reviews of Geophysics and Space Physics, **17**(6): 1155–1164.

Mitchell, J.K. 1993. Fundamentals of soil behavior. 2nd ed. John Wiley & Sons, Inc., New York.

Moore, C.A., and Mitchell, J.K. 1974. Electromagnetic forces and soil strength. Géotechnique, **24**(4): 627–640.

Santamarina, J.C., and Fam, M. 1995. Changes in dielectric permittivity and shear wave velocity during concentration diffusion. Canadian Geotechnical Journal, **32**(4): 647–659.

Santamarina, J.C., Klein, K.A., and Fam, M.A. 2001. Soils and waves. John Wiley & Sons Ltd., New York.

Sridharan, A., and Jayadeva, M.S. 1982. Double layer theory and compressibility of clays. Géotechnique, **32**(2): 133–144.

Sridharan, A., and Prakash, K. 1999. Mechanisms controlling the undrained shear strength behaviour of clays. Canadian Geotechnical Journal, **36**(6): 1030–1038.

Sridharan, A., and Venkatappa Rao, G. 1973. Mechanisms controlling volume change of saturated clays and the role of the effective stress concept. Géotechnique, **23**(3): 359–382.

Sridharan, A., and Venkatappa Rao, G. 1979. Shear strength behaviour of saturated clays and the role of the effective stress concept. Géotechnique, **29**(2): 177–193.

Ting, W.H. 1968. Some effects of history on the stress–strain behavior of kaolin. Ph.D. thesis, University of Cambridge, Cambridge, UK.

Vucetic, M., and Dobry, R. 1991. Effect of soil plasticity on cyclic response. Journal of Geotechnical Engineering, ASCE, **117**(1): 89–107.

Wang, Y.-H., and Siu, W.-K. 2006. Structure characteristics and mechanical properties of kaolinite soils. I. Surface charges and structural characterizations. Canadian Geotechnical Journal, **43**(3): 587–600.

Wheeler, S.J., and Sivakumar, V. 2000. Influence of compaction procedure on the mechanical behavior of an unsaturated compacted clay. Part 2: shearing and constitutive modeling. Géotechnique, **50**(4): 369–376.

Winkler, K., Nur, A., and Gladwin, M. 1979. Friction and seismic attenuation in rocks. Nature (London), **227**: 528–531.

Yao, M., and Anandarajah, A. 2003. Three-dimensional discrete element method of analysis of clays. Journal of Engineering Mechanics, ASCE, **129**(6): 585–596.